ALSAnchorNet: Biologically Informed Multimodal MRI Fusion for Amyotrophic Lateral Sclerosis Diagnosis

Xiongri Shen[1⋆], Jixin Luan[2,3⋆], Xingcan Hu[1], Le Lu[1], Fuchen Liu[2], Shuangwu Liu[2(✉)], and Long Xie[1(✉)]

[1] Ant Group, Hangzhou, Zhejiang, China
[2] Department of Neurology, Shandong Key Laboratory of Mitochondrial Medicine and Rare Diseases, Qilu Hospital of Shandong University, Jinan, Shandong, China
[3] Department of Radiology, Qilu Hospital of Shandong University, Jinan, Shandong, China
whuliushuangwu@163.com
long.xie@antgroup.com

Abstract. Deep learning–based multimodal MRI integration for Amyotrophic Lateral Sclerosis (ALS) diagnosis remains largely unexplored. We present **ALSAnchorNet**, a biologically guided multimodal framework that integrates resting-state fMRI, diffusion tensor imaging, and structural MRI for ALS diagnosis. We introduce Frontal Anchor Attention to encode frontal lobe vulnerability by using intra-frontal functional connectivity as an anchoring query to modulate whole-brain connectivity interactions. This anchor-guided mechanism enhances disease-relevant feature amplification during cross-modal fusion. ALSAnchorNet applies modality-specific linear projections followed by anchor-based refinement to jointly model connectivity, glymphatic, and cerebral-spinal fluid (CSF) markers. Using one of the largest ALS cohort to date of 159 ALS and 107 healthy controls, ALSAnchorNet achieves 77% classification accuracy with AUC = 0.80, outperforming single-modality models and non-anchored fusion approaches. Ablation analyses demonstrate that glymphatic and CSF markers provide complementary diagnostic value beyond connectivity features. Interpretability analysis further reveals elevated contributions from the superior frontal gyri and paracentral lobule, consistent with established motor network involvement in ALS. These results establish an important first step toward biologically grounded deep learning for multimodal ALS modeling. Future work will incorporate biofluid markers and longitudinal data for more comprehensive disease modeling.

Keywords: Amyotrophic lateral sclerosis · Multi-modal MRI diagnosis

1 Introduction

Amyotrophic lateral sclerosis (ALS) is a multi-system neurodegenerative disorder associated with high morbidity and mortality [18]. Multimodal magnetic reso-

⋆ Xiongri Shen and Jixin Luan contributed equally to this work.

nance imaging (MRI) provides complementary structural and functional measurements that have shown promise for biomarker discovery in neurodegenerative diseases, including early detection of Alzheimer's disease [26]. However, progress in ALS neuroimaging biomarker development has been hindered by limited large-scale multimodal MRI datasets and the absence of principled integration frameworks. As a result, most prior ALS neuroimaging studies rely on population-level statistical analyses using single modalities, including structural MRI (sMRI) [25,10], diffusion tensor imaging (DTI) [13], and resting-state fMRI (rs-fMRI) [21], limiting translational utility for subject-level diagnosis.

Although traditional machine learning approaches have attempted multimodal fusion [4,9], their limited representational capacity and poor generalization restrict clinical applicability, particularly in small and heterogeneous cohorts, where most prior studies include fewer than 100 ALS patients. In contrast, deep learning has achieved state-of-the-art performance in large-scale neuroimaging studies of Alzheimer's and Parkinson's disease using convolutional neural networks (CNNs), graph convolutional networks (GCNs), and Transformer-based architectures [2,12,11]. Yet, such advances remain largely unexplored in ALS.

Here, we leverage one of the largest multimodal MRI ALS cohorts to date (159 ALS patients, 107 controls) to develop a biologically grounded deep learning framework. A central focus of this work is the optimized extraction of ALS-relevant features from high-dimentional functional and structural connectomes (FC/SC). Crucially, we argue that existing multimodal models overlook disease-specific neuroanatomical priors. ALS exhibits early frontal lobe vulnerability [13,10], but prior architectures treat brain connectivity as generic graphs or images. Even recent attention-based models [24] rely on heavy cross-attention or graph modules, introducing substantial parameter overhead and overfitting risk in data-limited settings. To address this gap, we propose a *neuroanatomically anchored*, *parameter-efficient* fusion strategy that explicitly encodes frontal lobe vulnerability into the model architecture. Rather than increasing model complexity, we inject biological prior knowledge through a lightweight anchor attention mechanism that selectively modulates connectivity representations. In addition to FC and SC, we incorporate MRI-extracted glymphatic and cerebral-spinal fluid (CSF) biomarkers (see Sec. 2), enabling system-level characterization of ALS pathology within a unified multimodal framework.

In this work, main contributions are three-fold. 1) We introduce **ALSAnchorNet**, a biologically informed multimodal deep learning framework that integrates connectivity, glymphatic, and CSF biomarkers, achieving 77% classification accuracy with AUC = 0.80, establishing state-of-the-art performance for multimodal MRI-based ALS diagnosis. 2) We propose **Frontal Anchor Attention (FAA)**, a disease-guided attention mechanism that leverages intra-frontal connectivity to modulate whole-brain interactions. This design improves diagnostic accuracy and interpretability while remaining parameter-efficient compared to Transformer-based fusion. Interpretability analysis further reveals motor network vulnerability consistent with ALS literature. 3) We provide a processed multimodal MRI ALS dataset to support future development and validation of

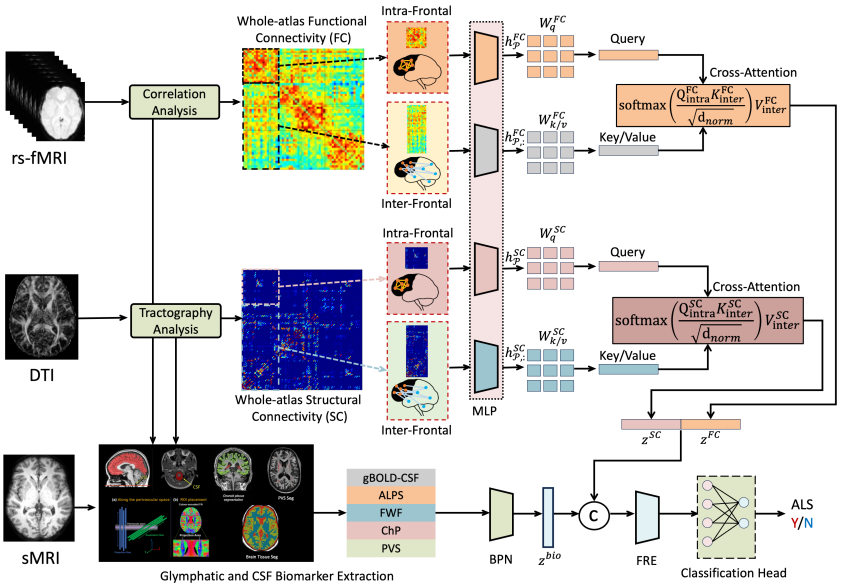

Fig. 1: Overview of the proposed **ALSAnchorNet** framework. (1) Functional and structural connectivity matrices (60,516-dim each) are encoded via modality-specific MLPs with ReLU and dropout. (2) The *Frontal Anchor Attention* (FAA) module uses intra-frontal connections as queries to attend over frontal-to-whole-brain interactions, yielding neuroanatomically informed connectivity embeddings. (3) Multimodal glymphatic and CSF biomarkers (PVS, ChP, ALPS, FWF, gBOLD–CSF; 93-dim) are projected via a Biomarker Projection Network (BPN). (4) Connectivity, glymphatic and CSF biomarker features are concatenated and refined through a Fusion Refinement Encoder (FRE) before final ALS vs. HC classification.

imaging biomarkers for ALS. The code is available at `https://github.com/AQ-MedAI/ALSAnchorNet`.

2 Dataset and Preprocessing

Our cohort comprises 266 participants recruited from Qilu Hospital, including 159 patients with ALS and 107 age-matched healthy controls (HC). All participants were scanned on a 3T MRI system with rs-fMRI, DTI, and sMRI acquired. The study was approved by the institutional ethics committee, and written informed consent was obtained from all participants. Image preprocessing followed established pipelines. Structural MRI was processed using FreeSurfer v6.0. DTI data underwent `eddy` and `topup` correction, followed by diffusion modeling. rs-fMRI preprocessing included motion regression, band-pass filtering (0.01–0.1 Hz), and global signal regression. The following disease-related measures were then extracted:

- **Functional/Structural Connectivity (FC/SC)**: Functional connectivity matrices were computed from rs-fMRI using the BrainNetome Atlas (BNA) [8]. Structural connectivity matrices were constructed via probabilistic tractography using PANDA on DTI data [5].
- **Enlarged Perivascular Spaces (PVS, d = 6)**: PVS has been shown to be associated with ALS in prior study [16]. PVS measurements were extracted from sMRI using a validated pipeline based on the Frangi filter [14].
- **Glymphatic and CSF biomarkers**: Increasing evidence suggests that impaired glymphatic clearance and CSF dynamics may contribute to neurodegeneration including ALS. Therefore, we extracted the following markers:
  - **Peri-cortical free water fraction (FWF, d = 70)** derived from DTI, quantifying extracellular free water in peri-cortical regions. Elevated FWF has been associated with altered interstitial fluid exchange and neuroinflammatory processes [27].
  - **DTI Analysis along the Perivascular Space (ALPS, d = 11)**, computed from diffusion anisotropy along medullary vein–aligned projection and association fibers, providing an indirect proxy of perivascular fluid transport efficiency [20].
  - **gBOLD–CSF coupling (d = 3)**, estimated from rs-fMRI as the temporal correlation between global BOLD signal fluctuations and CSF signal changes, reflecting neurovascular–CSF interaction dynamics [17].
  - **Choroid Plexus (ChP) volume (d = 3)**, extracted from sMRI, serving as a marker of CSF production and blood–CSF barrier integrity [6].

3 Method

We propose **ALSAnchorNet**, a biologically informed neural network for ALS classification that integrates brain connectivity with glymphatic and CSF biomarkers. Let $\mathbf{a}^{\mathrm{FC}}, \mathbf{a}^{\mathrm{SC}} \in \mathbb{R}^{d_c}$ denote the vectorized FC and SC matrices ($d_c = 60,516$), and $\mathbf{x}^{\mathrm{bio}} \in \mathbb{R}^{d_b}$ the multimodal vector comprising PVS, ALPS, ChP, FWF, gBOLD-CSF ($d_b = 93$).

Frontal Anchor Attention (FAA). Let $\mathcal{P} \subset \{1, \ldots, N\}$ index the frontal lobe regions [e.g., superior frontal gyrus (SFG), middle frontal gyrus (MFG); $|\mathcal{P}| = 68$]. We partition the connectivity embeddings into the *intra-frontal* subvector $\mathbf{a}_{\mathcal{P}}$ (internal connections) and the *inter-frontal* subvector $\mathbf{a}_{\mathcal{P},:}$ (connections to the whole brain). We then encode these intra- and inter-frontal subvectors of FC and SC using separate multi-layer perceptrons (MLPs):

$$\mathbf{h}^{\mathrm{FC}}_{\mathcal{P}} = \phi_{\mathrm{enc}}(\mathbf{a}^{\mathrm{FC}}_{\mathcal{P}}), \mathbf{h}^{\mathrm{FC}}_{\mathcal{P},:} = \phi_{\mathrm{enc}}(\mathbf{a}^{\mathrm{FC}}_{\mathcal{P},:}), \mathbf{h}^{\mathrm{SC}}_{\mathcal{P}} = \phi_{\mathrm{enc}}(\mathbf{a}^{\mathrm{SC}}_{\mathcal{P}}), \mathbf{h}^{\mathrm{SC}}_{\mathcal{P},:} = \phi_{\mathrm{enc}}(\mathbf{a}^{\mathrm{SC}}_{\mathcal{P},:}) \quad (1)$$

where $\phi_{\mathrm{enc}}(\cdot)$ = MLP with ReLU and dropout.

Then, we construct FS or SC queries, keys, and values with explicit regional indicators:

$$\mathbf{Q}^{\mathrm{FC}}_{\mathrm{intra}} = \mathbf{W}^{\mathrm{FC}}_{q}\mathbf{h}^{\mathrm{FC}}_{\mathcal{P}} \in \mathbb{R}^{d_q}, \qquad \mathbf{Q}^{\mathrm{SC}}_{\mathrm{intra}} = \mathbf{W}^{\mathrm{SC}}_{q}\mathbf{h}^{\mathrm{SC}}_{\mathcal{P}} \in \mathbb{R}^{d_q}, \quad (2)$$

$$\mathbf{K}^{\mathrm{FC}}_{\mathrm{inter}} = \mathbf{W}^{\mathrm{FC}}_{k}\mathbf{h}^{\mathrm{FC}}_{\mathcal{P},:} \in \mathbb{R}^{d_{kv}}, \qquad \mathbf{K}^{\mathrm{SC}}_{\mathrm{inter}} = \mathbf{W}^{\mathrm{SC}}_{k}\mathbf{h}^{\mathrm{SC}}_{\mathcal{P},:} \in \mathbb{R}^{d_{kv}}, \quad (3)$$

$$\mathbf{V}^{\mathrm{FC}}_{\mathrm{inter}} = \mathbf{W}^{\mathrm{FC}}_{v}\mathbf{h}^{\mathrm{FC}}_{\mathcal{P},:} \in \mathbb{R}^{d_{kv}}, \qquad \mathbf{V}^{\mathrm{SC}}_{\mathrm{inter}} = \mathbf{W}^{\mathrm{SC}}_{v}\mathbf{h}^{\mathrm{SC}}_{\mathcal{P},:} \in \mathbb{R}^{d_{kv}}. \quad (4)$$

Subsequently, we compute the attended connectivity representations for each modality by matching intra-frontal queries with inter-frontal contexts:

$$\mathbf{z}^{\mathrm{FC}} = \mathrm{softmax}\left(\frac{\mathbf{Q}^{\mathrm{FC}}_{\mathrm{intra}}(\mathbf{K}^{\mathrm{FC}}_{\mathrm{inter}})^{\top}}{\sqrt{d_{norm}}}\right)\mathbf{V}^{\mathrm{FC}}_{\mathrm{inter}}, \tag{5}$$

$$\mathbf{z}^{\mathrm{SC}} = \mathrm{softmax}\left(\frac{\mathbf{Q}^{\mathrm{SC}}_{\mathrm{intra}}(\mathbf{K}^{\mathrm{SC}}_{\mathrm{inter}})^{\top}}{\sqrt{d_{norm}}}\right)\mathbf{V}^{\mathrm{SC}}_{\mathrm{inter}}, \tag{6}$$

Here, the subscripts 'intra' and 'inter' explicitly denote features derived from internal frontal connectivity and frontal-to-whole-brain connectivity, respectively. This design enables ALSAnchorNet to use frontal lobe integrity (intra) to attend to distributed network disruptions (inter) in a modality-specific manner.

Biomarker Projection Network (BPN). The glymphatic and CSF biomarker vector is projected to a compact space:

$$\mathbf{z}^{\mathrm{bio}} = \mathrm{ReLU}\big(\mathbf{W}_b\mathbf{x}^{\mathrm{bio}} + \mathbf{b}_b\big), \quad \mathbf{W}_b \in \mathbb{R}^{d_z \times d_b} \tag{7}$$

Fusion and Refinement. We concatenate the three streams and refine via a fusion encoder:

$$\mathbf{z}^{\mathrm{fuse}} = [\mathbf{z}^{\mathrm{FC}}; \mathbf{z}^{\mathrm{SC}}; \mathbf{z}^{\mathrm{bio}}] \in \mathbb{R}^{2d_v + d_z}, \tag{8}$$

$$\mathbf{z}^{\mathrm{final}} = \psi_{\mathrm{refine}}(\mathbf{z}^{\mathrm{fuse}}), \tag{9}$$

where $\psi_{\mathrm{refine}}(\cdot) = \mathrm{MLP}_{(2d_v+d_z)\to d_f}$ implements the *Fusion Refinement Encoder (FRE)* to highlight discriminative cross-modal interactions.

The final prediction is obtained by:

$$\hat{y} = \mathrm{softmax}\big(\psi_{\mathrm{classifier}}(\mathbf{z}^{\mathrm{final}})\big) \tag{10}$$

where $\psi_{\mathrm{classifier}} = \mathrm{MLP}_{d_f \to 2}$.

The model is trained end-to-end with cross-entropy loss. By anchoring attention on the frontal lobe—a region critically affected in ALS—ALSAnchorNet enforces biologically plausible feature learning while enabling flexible multimodal integration through hierarchical linear projections.

Implementation Details. ALSAnchorNet is implemented in PyTorch on A100 GPUs by NVIDIA. FC/SC inputs (60,516-dim, 246-region atlas) are processed by frontal MLP extractors separating internal (68×68) and external (68×178) frontal connections. AttentionFusion modules use intra-frontal connectivity as queries to modulate whole-brain interactions (hidden dim=256). Multimodal biomarkers (93-dim: ALPS, ChP, FWF, gBOLD–CSF, PVS) are encoded via linear MLP (BPN, 256→128→64). FRE consists of MLP (576→256→128), followed by classifier (128→64→2). Training: 100 epochs, batch=16, Adam (lr=1×10^{-4}, weight decay=1×10^{-5}), early stopping (patience=15), seed=42. LayerNorm applied to all inputs; dropout=0.3 throughout. Five-fold cross-validation stratified by class is performed and averaged metrices are reported.

4 Results

4.1 Classification Performance

We evaluate the proposed **ALSAnchorNet** against a range of baseline models under two experimental settings (Table 1). In the first setting, only functional and structural connectivity (FC/SC) features are used. Among existing methods, GCN achieves the highest accuracy (0.66) but suffers from low AUC (0.58), indicating sensitivity to class imbalance. Our intermediate module, *FAA*—which leverages frontal lobe centric cross-regional attention—outperforms all baselines, achieving 0.70 accuracy and 0.68 AUC, demonstrating the value of neuroanatomical priors.

Table 1: Performance comparison of different methods on the ALS classification task. Standard deviations across five folds in parentheses. Top: using only FC/SC. Bottom: using all seven multimodal features. T/C/G denotes Transformer/CNN/GNN.

Method	**AUC**	**Acc**	**Precision**	**Recall**	**F1**
			Using FC/SC		
SVM-Chen et al.[4]	0.43(0.06)*	0.58(0.01)*	0.50(0.08)*	0.50(0.01)*	0.46(0.05)*
Cluster-Milella et al.[19]	–	0.55	–	–	–
CNN-Erdaş et al.[3]	0.54(0.03)*	0.63(0.01)*	0.63(0.01)	1.00(0.00)*	0.77(0.01)*
GCN-Devipriya et al.[7]	0.58(0.09)	0.66(0.01)*	0.63(0.10)	1.00(0.01)*	0.77(0.07)*
C+T-Asuai et al.[1]	0.62(0.05)	0.62(0.04)*	0.62(0.03)*	1.00(0.01)*	0.76(0.07)*
G+T-Shang et al.[23]	0.54(0.07)*	0.61(0.04)*	0.63(0.13)	0.91(0.10)*	0.73(0.10)
ResNet-Rahman et al.[22]	0.62(0.06)	0.65(0.03)*	0.66(0.07)	0.65(0.06)	0.66(0.06)
ViT-Kushol et al.[15]	0.62(0.05)	0.58(0.05)*	0.65(0.03)	0.66(0.15)	0.65(0.07)
FAA (ours)	0.68(0.07)	0.70(0.03)	0.70(0.07)	0.70(0.06)	0.67(0.06)
			Using all fused multimodal features		
CNN-Erdaş et al.[3]	0.68(0.06)	0.74(0.01)	0.81(0.01)	0.74(0.11)	0.69(0.05)
GCN-Devipriya et al.[7]	0.70(0.04)	0.64(0.05)†	0.67(0.06)	0.64(0.05)†	0.64(0.07)
Transformer	0.66(0.10)	0.64(0.04)†	0.67(0.03)	0.64(0.04)†	0.64(0.04)†
ALSAnchorNet (ours)	**0.80(0.11)**	**0.77(0.05)**	**0.77(0.13)**	**0.77(0.05)**	**0.77(0.11)**

Note: * Indicates a statistically significant difference from the corresponding metric of FAA. † Indicates a statistically significant difference from the corresponding metric of ALSAnchorNet. Two-sided Student's t-tests were used.

In the second setting, all seven multimodal biomarkers (FC, SC, PVS, ChP, ALPS, gBOLD–CSF, FWF) are used as input. The CNN baseline shows substantial gains (accuracy: 0.74, precision: 0.81), confirming that glymphatic and CSF markers enhance diagnostic power. Notably, our full **ALSAnchorNet** achieves state-of-the-art performance with balanced metrics across the board: accuracy = 0.77, precision = 0.77, recall = 0.77, F1 = 0.77, and AUC = 0.80, establishing a new benchmark for multimodal ALS vs. HC classification.

Table 2: Ablation study of ALSAnchorNet: (a) feature modality contributions and (b) architectural component effectiveness.

Configuration	AUC	Acc	Precision	Recall	F1
(a) Feature Modality Ablation					
FC + SC only	0.69	0.63	0.63	1.00	0.77
Glymphatic and CSF markers only†	0.66	0.67	0.65	0.67	0.63
All modalities (Full)	**0.80**	**0.77**	**0.77**	**0.77**	**0.77**
(b) Architectural Component Ablation					
MLP fusion (baseline)	0.54	0.63	0.63	1.00	0.77
+ Frontal Anchor Attention (FAA)	0.68	0.70	0.70	0.70	0.67
Full ALSAnchorNet	**0.80**	**0.77**	**0.77**	**0.77**	**0.77**

Note: † Glymphatic and CSF markers: PVS, ChP, ALPS, gBOLD–CSF, FWF.

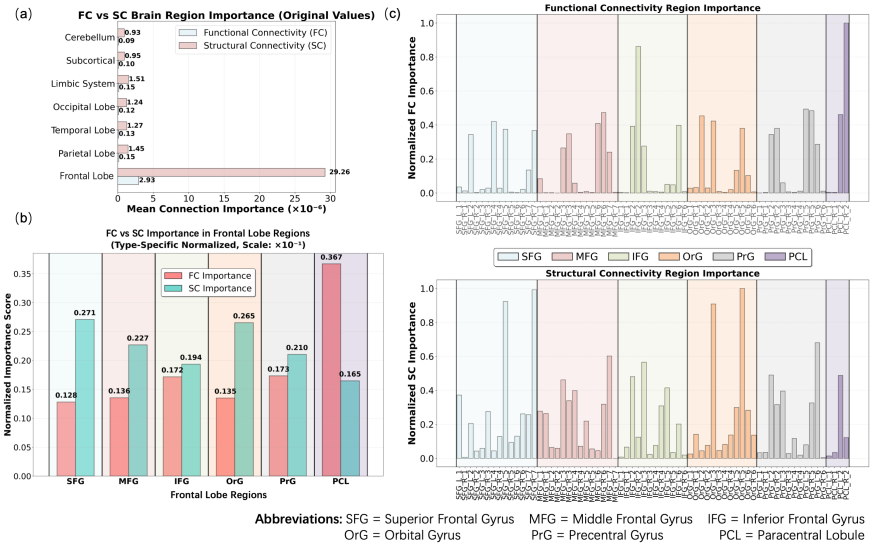

Fig. 2: **Interpretability analysis of brain-wise and frontal-specific contributions.** (**a**) Modality-specific contribution scores across brain regions of the BrainNetome Atlas, comparing Functional (FC) and Structural (SC) connectivity. (**b**) Focused comparison of FC and SC scores restricted to *frontal lobe subregions*. (**c**) High-resolution breakdown of importance scores for the 68 individual frontal lobe subregions, highlighting dominant areas such as PCL.

4.2 Ablation Studies

Modality Ablation. To quantify biomarker contributions, we performed modality ablation on ALSAnchorNet. While FC/SC alone yielded 0.63 accuracy, the five non-connectivity biomarkers (PVS, ChP, ALPS, gBOLD–CSF, FWF) achieved higher accuracy (0.67), highlighting the relevance of glymphatic/CSF dysfunction. Combining all seven features delivered the best performance (accuracy: 0.77, AUC: 0.80), confirming their complementary nature.
Model Component Ablation. Dissecting ALSAnchorNet's architecture, a simple concatenation baseline achieved 0.63 accuracy but suffered recall bias (recall=1.00). Replacing this with *Frontal Anchor Attention* (FAA) improved balance and performance (0.70 accuracy, 0.68 AUC). The full pipeline, integrating biomarker projection, FAA, and fusion refinement, yielded consistent gains across all metrics (0.77 accuracy, 0.8 AUC), validating each design choice.

4.3 Interpretability Analysis

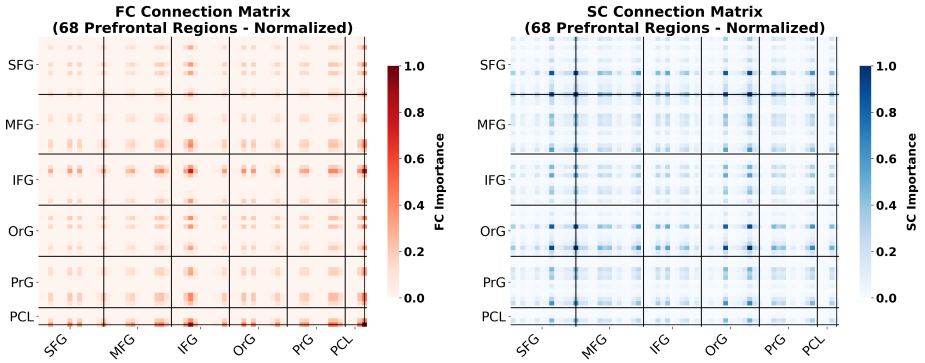

Fig. 3: Gradient-based importance heatmaps of **intra-frontal connectivity** (68×68 matrices) for FC and SC modalities. Brighter regions indicate stronger diagnostic contributions. The patterns reveal discriminative interaction pathways within sensorimotor network (SMN, PCL–PCL connections), aligning with ALS-related motor network vulnerability.

To assess biological plausibility, we visualized region-specific contributions and intra-frontal connectivity patterns using gradient-based attribution (Figs. 2–3). The paracentral lobule (PCL) and superior frontal gyrus (SFG)—regions critical for lower-limb motor–sensory function and motor planning—exhibit elevated importance scores in FC and SC, respectively (Figs. 2b). Beyond regional effects, connectivity heatmaps (Fig. 3) demonstrate increased weights within the sensorimotor network (SMN), particularly within the PCL. These high-importance connections are consistent with the strongest gradient signals identified in our

attribution analysis and align with known patterns of motor network vulnerability in ALS [21]. Collectively, these results indicate that ALSAnchorNet not only achieves good diagnostic performance, but also learns clinically meaningful and neuroanatomically coherent representations.

5 Conclusion

We propose **ALSAnchorNet**, a biologically grounded framework for ALS diagnosis that integrates connectomic, glymphatic and CSF biomarkers from multimodal MRI via Frontal Anchor Attention (FAA). Our model achieves 77% classification accuracy with AUC=0.80, outperforming connectivity-only and non-anchored baselines. These results represent an important first step toward biologically informed deep learning for multimodal ALS modeling—an area that remains largely underexplored despite its potential to better capture the heterogeneity of the disease. By explicitly incorporating disease-specific neuroanatomical priors, our approach demonstrates that principled architectural design can improve both performance and interpretability. This study has several limitations, including a single-center cohort and cross-sectional design, which may limit generalizability. Future work will extend the framework to multi-center validation, longitudinal modeling, and integration of biofluid biomarkers to enable more comprehensive and personalized characterization of ALS.

Disclosure of Interests. Authors Xiongri Shen, Xingcan Hu, Le Lu, and Long Xie are employees of Ant Group.

References

1. Asuai, C., Andrew, M., Arinomor, A.P., Ogheneochuko, D.E., Joseph-Brown, A.A., Merit, I., Collins, A.: Transformer-augmented deep learning ensemble for multimodal neuroimaging-based diagnosis of amyotrophic lateral sclerosis. Journal of Computing Theories and Applications **3**(2), 190–205 (2025)
2. Bannadabhavi, A., Lee, S., Deng, W., Ying, R., Li, X.: Community-aware transformer for autism prediction in fmri connectome. In: International conference on medical image computing and computer-assisted intervention. pp. 287–297. Springer (2023)
3. Berke Erdaş, Ç., Sümer, E., Kibaroğlu, S.: Cnn-based severity prediction of neurodegenerative diseases using gait data. Digital Health **8**, 20552076221075147 (2022)
4. Chen, H., Hu, Z., Ke, Z., Xu, Y., Bai, F., Liu, Z.: Aberrant multimodal connectivity pattern involved in default mode network and limbic network in amyotrophic lateral sclerosis. Brain Sciences **13**(5), 803 (2023)
5. Cui, Z., Zhong, S., Xu, P., He, Y., Gong, G.: Panda: a pipeline toolbox for analyzing brain diffusion images. Frontiers in human neuroscience **7**, 42 (2013)
6. Dai, T., Lou, J., Kong, D., Li, J., Ren, Q., Chen, Y., Sun, S., Yun, Y., Sun, X., Yang, Y., et al.: Choroid plexus enlargement in amyotrophic lateral sclerosis patients and its correlation with clinical disability and blood-csf barrier permeability. Fluids and Barriers of the CNS **21**(1), 36 (2024)

7. Devipriya, S., Vijaya, M.: Graph convolutional neural network for ic50 prediction model using amyotrophic lateral sclerosis targets. In: International Conference on Data Science and Applications. pp. 77–91. Springer (2023)
8. Fan, L., Li, H., Zhuo, J., Zhang, Y., Wang, J., Chen, L., Yang, Z., Chu, C., Xie, S., Laird, A.R., et al.: The human brainnetome atlas: a new brain atlas based on connectional architecture. Cerebral cortex **26**(8), 3508–3526 (2016)
9. Ferraro, P.M., Agosta, F., Riva, N., Copetti, M., Spinelli, E.G., Falzone, Y., Sorarù, G., Comi, G., Chiò, A., Filippi, M.: Multimodal structural mri in the diagnosis of motor neuron diseases. NeuroImage: Clinical **16**, 240–247 (2017)
10. Grosskreutz, J., Kaufmann, J., Frädrich, J., Dengler, R., Heinze, H.J., Peschel, T.: Widespread sensorimotor and frontal cortical atrophy in amyotrophic lateral sclerosis. BMC neurology **6**(1), 17 (2006)
11. Ibrahim, B., Suppiah, S., Ibrahim, N., Mohamad, M., Hassan, H.A., Nasser, N.S., Saripan, M.I.: Diagnostic power of resting-state fmri for detection of network connectivity in alzheimer's disease and mild cognitive impairment: A systematic review. Human brain mapping **42**(9), 2941–2968 (2021)
12. Jiang, H., Cao, P., Xu, M., Yang, J., Zaiane, O.: Hi-gcn: A hierarchical graph convolution network for graph embedding learning of brain network and brain disorders prediction. Computers in Biology and Medicine **127**, 104096 (2020)
13. Kalra, S., Müller, H.P., Ishaque, A., Zinman, L., Korngut, L., Genge, A., Beaulieu, C., Frayne, R., Graham, S.J., Kassubek, J.: A prospective harmonized multicenter dti study of cerebral white matter degeneration in als. Neurology **95**(8), e943–e952 (2020)
14. Kamagata, K., Andica, C., Takabayashi, K., Saito, Y., Taoka, T., Nozaki, H., Kikuta, J., Fujita, S., Hagiwara, A., Kamiya, K., et al.: Association of mri indices of glymphatic system with amyloid deposition and cognition in mild cognitive impairment and alzheimer disease. Neurology **99**(24), e2648–e2660 (2022)
15. Kushol, R., Luk, C.C., Dey, A., Benatar, M., Briemberg, H., Dionne, A., Dupré, N., Frayne, R., Genge, A., Gibson, S., et al.: Sf2former: Amyotrophic lateral sclerosis identification from multi-center mri data using spatial and frequency fusion transformer. Computerized Medical Imaging and Graphics **108**, 102279 (2023)
16. Lee, B.C., Kuo, Y.C., Cheng, L.F., Tsai, Y.C., Huang, J.Z., Tsai, H.H., Lin, J.S., Huang, P.Y., Ting, C.H., Yang, C.C., et al.: The significance and mechanism of cerebral enlarged perivascular space in amyotrophic lateral sclerosis. International Journal of Molecular Sciences **26**(19), 9474 (2025)
17. Liu, Z., Dong, H., Yang, H., Zhou, L., Li, M., Zhang, X., Zhao, Y., Han, M., Liu, Y., Geng, Z.: Glymphatic dysfunction in amyotrophic lateral sclerosis: a multimodal mri investigation of brain-csf functional and structural dynamics. Frontiers in Neuroscience **19**, 1666114 (2025)
18. Masrori, P., Van Damme, P.: Amyotrophic lateral sclerosis: a clinical review. European journal of neurology **27**(10), 1918–1929 (2020)
19. Milella, G., Zoccolella, S., Giugno, A., Filardi, M., Urso, D., Nigro, S., Tafuri, B., Tamburrino, L., Gnoni, V., Logroscino, G.: The impact of upper and lower motor neuron burden on diagnostic certainty, and clinical course of spinal-onset amyotrophic lateral sclerosis: a cluster-based approach. Journal of Neurology **270**(10), 4868–4875 (2023)
20. Ni, C., Chen, L., Lin, R., Zheng, W.Y., Cai, Y., Cai, G., Zeng, Y., Ye, Q., Jiang, R., Wáng, Y.X.J.: Diffusion tensor image analysis along the perivascular space and quantitative susceptibility mapping in the diagnosis and severity assessment of parkinson's disease. Quantitative Imaging in Medicine and Surgery **15**(2), 1411 (2025)

21. Proudfoot, M., Bede, P., Turner, M.R.: Imaging cerebral activity in amyotrophic lateral sclerosis. Frontiers in neurology **9**, 1148 (2019)
22. Rahman, K., Shair, E., Abdullah, A., Lee, T., Nazm, N.: Deep learning classification of gait disorders in neurodegenerative diseases among older adults using resnet-50. International Journal of Advanced Computer Science & Applications **15**(11) (2024)
23. Shang, H., Xu, W., Zhu, H., Zang, X., Qiao, J.: Gctn: A novel graph convolutional and transformer-based network for multimodal neuroimaging analysis and neurodegenerative disease classification. In: Proceedings of the 2024 5th International Symposium on Artificial Intelligence for Medicine Science. pp. 667–671 (2024)
24. Shen, X., Song, Z., Zhang, Z.: Gcan: Generative counterfactual attention-guided network for explainable cognitive decline diagnostics based on fmri functional connectivity. In: International Conference on Medical Image Computing and Computer-Assisted Intervention. pp. 416–426. Springer (2024)
25. Steinbach, R., Prell, T., Gaur, N., Roediger, A., Gaser, C., Mayer, T.E., Witte, O.W., Grosskreutz, J.: Patterns of grey and white matter changes differ between bulbar and limb onset amyotrophic lateral sclerosis. NeuroImage: Clinical **30**, 102674 (2021)
26. Veitch, D.P., Weiner, M.W., Miller, M., Aisen, P.S., Ashford, M.A., Beckett, L.A., Green, R.C., Harvey, D., Jack Jr, C.R., Jagust, W., et al.: The alzheimer's disease neuroimaging initiative in the era of alzheimer's disease treatment: a review of adni studies from 2021 to 2022. Alzheimer's & Dementia **20**(1), 652–694 (2024)
27. Zhang, J., Yang, X., Wang, Y., Xu, X., Zheng, Y., Huang, Q., Wang, W., Xu, W., Guan, Y., Liu, J., et al.: Identifying distinct spatiotemporal patterns of juxtacortical microstructure in alzheimer disease using diffusion mri–derived free water fraction. Radiology **317**(1), e243423 (2025)